ACS APPLIED MATERIALS & INTERFACES

Research Article

www.acsami.org

Improved Electrical Conductivity of Polyamide 12/Graphene Nanocomposites with Maleated Polyethylene-Octene Rubber Prepared by Melt Compounding

Dong Yan,[†] Hao-Bin Zhang,[†] Yu Jia,[‡,§] Juan Hu,[†] Xian-Yong Qi,[†] Zhong Zhang,*[,‡] and Zhong-Zhen Yu*[,†]

[†]State Key Laboratory of Organic−Inorganic Composites, Department of Polymer Engineering, College of Materials Science and Engineering, Beijing University of Chemical Technology, Beijing 100029, China

[‡]National Center for Nanoscience and Technology, Beijing 100190, China

[§]Department of Modern Mechanics, University of Science and Technology of China, Hefei 230027, China

ABSTRACT: Electrically conductive polyamide 12 (PA12)/graphene binary nanocomposites with a low percolation threshold of 0.3 vol % were prepared by melt compounding. A rapid increase in electrical conductivity from 2.8×10^{-14} S/m of PA12 to 6.7×10^{-2} S/m was achieved with ~1.38 vol % graphene. It is shown that graphene sheets were homogeneously dispersed in PA12 matrix. Furthermore, polyethylene-octene rubber grafted with maleic anhydride (POE-g-MA) was used to further enhance the electrical conductivity of PA12/graphene nanocomposites. Three compounding sequences were adopted to tailor the microstructure and properties of the ternary nanocomposites. Both highest electrical conductivity and storage modulus were obtained when most graphene sheets were located in PA12 matrix rather than in POE-g-MA phase.

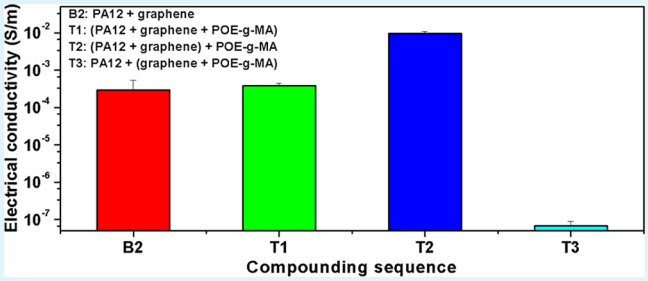

KEYWORDS: *polyamide 12, graphene, melt compounding, electrical conductivity, selective localization, nanocomposites*

INTRODUCTION

Graphene has recently attracted much attention from both the scientific and industrial communities because of its superior electrical, thermal and mechanical properties.[1−6] In particular, its high aspect ratio and electrical conductivity make it very effective in endowing electrical and electromagnetic interference shielding properties to insulating polymers.[5,7−9] Stankovich et al. prepared electrically conductive polystyrene/graphene nanocomposites by solution mixing, resulting in a low percolation threshold of 0.1 vol %.[10] Compared to solution mixing, however, melt compounding is an eco-friendly approach to prepare conductive polymer nanocomposites because melt compounding process is more compatible with conventional polymer processing facilities and readily produces high performance polymer nanocomposites in commercial scale.[4,5,11−17] By melt compounding, we obtained electrically conductive polyethylene terephthalate/graphene nanocomposites with a low electrical percolation threshold of 0.47 vol %,[5] lower than many carbon nanotubes filled polymer nanocomposites that were also prepared by melt compounding.[18−20] Melt-compounded polyester and polyurethane nanocomposites filled with graphene were also shown lower percolation thresholds than 0.5 vol %.[4,21]

However, the disadvantage of melt compounding is that the strong shearing force would decrease the aspect ratios of anisotropic nanofillers (such as graphene and carbon nanotubes) and thus high loading of the nanofillers is required to form an interconnected conducting network in polymer matrices, which would unavoidably deteriorate ductility, toughness and melt processability of polymers. To address this problem, the second polymer phase is generally incorporated into the binary polymer composites to further enhance the electrical and mechanical properties.[12,22−28] Recently, Yang et al. reported the simultaneous enhancement of electrical conductivity and impact strength by adding ethylene-propylene-diene ternary rubber (EPDM) in polypropylene/carbon black composites. By a two-step compounding approach, carbon black particles were selectively distributed around EPDM phase, which significantly decreased the percolation threshold and improved the impact strength.[27] In our recent work,[12] maleic anhydride grafted polyethylene-octene rubber (POE-g-MA) was incorporated with polyamide 6 (PA6)/multiwalled carbon nanotube (MWNT) components to improve both electrical conductivity and toughness of the nanocomposite. With MWNTs selectively locating in PA6 phase, the electrical conductivity was higher in the ternary nanocomposite than that of its corresponding binary nanocomposite because of the "volume-exclusion" effect of POE-g-

Received: June 21, 2012
Accepted: August 13, 2012
Published: August 13, 2012

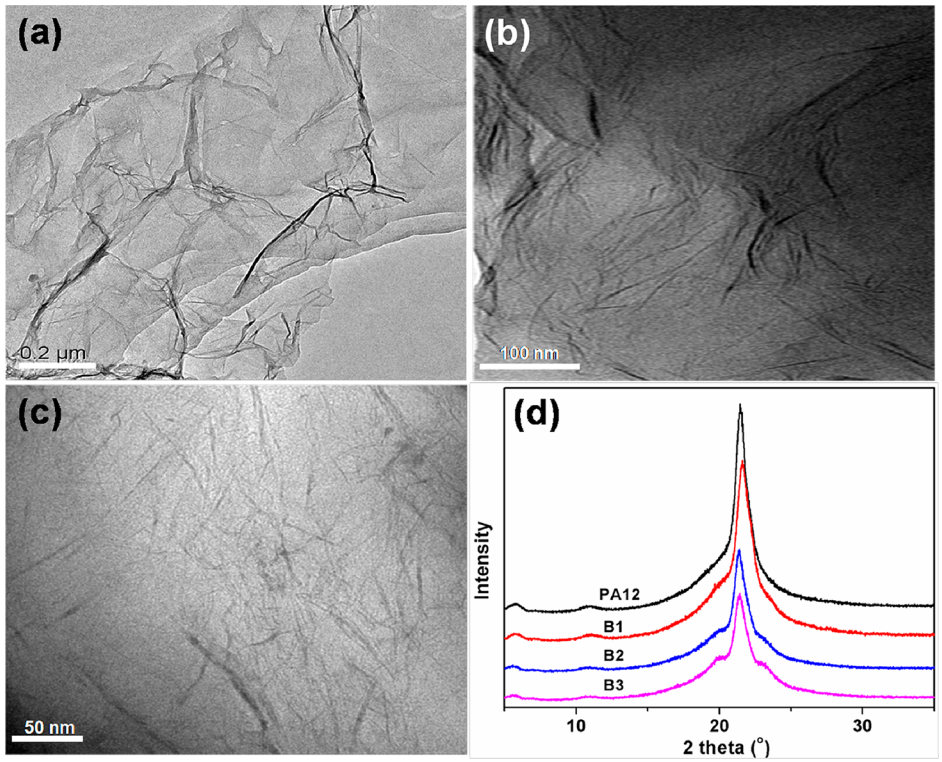

Figure 1. (a) TEM micrograph of graphene; (b, c) TEM micrographs of PA12 nanocomposite with 2 wt % graphene; (d) XRD patterns of PA12 and its nanocomposites with (B1) 1, (B2) 2, and (B3) 3 wt % graphene.

MA. Here, we first prepared electrically conductive polyamide 12 (PA12)/graphene nanocomposites by melt compounding with a focus on their morphology and electrical properties. Subsequently, POE-g-MA was introduced as the second polymer phase to improve the electrical conductivity and toughness, the microstructure and properties were optimized by varying the compounding sequences of PA12, graphene, and POE-g-MA components.

EXPERIMENTAL SECTION

2.1. Materials. PA12 with a trade name of Vestamid L1700 was obtained from Degussa, Germany. Its density and number-average molecular weight are 1.02 g/cm^3 and 2.5 × 10^4 g/mol, respectively. Polyethylene-octene rubber with 1 wt % maleic anhydride (POE-g-MA) was supplied by Haier Kehua Co. Ltd. (Beijing, China). Pristine graphite flakes with a mean size of 48 μm were provided by Huadong Graphite Factory (China). Concentrated sulphuric acid (95−98%), fuming nitric acid (85%), hydrochloric acid (37%) and potassium chlorate (98%) were bought from Beijing Chemical Factory (China) and used as received.

2.2. Preparation of Graphene. Graphite oxide was prepared by oxidizing pristine graphite according to the Staudenmaier method.[29,30] First, graphite flakes (5 g) were added to the mixture of concentrated sulphuric acid (87.5 mL) and fuming nitric acid (45 mL) with vigorous stirring. Potassium chlorate (55 g) was then added into the suspension slowly. After reacting for 96 h at room temperature, graphite oxide was obtained by centrifuging with a Shanghai Anting TDL-40B high-speed centrifuge (China) and dried in a vacuum oven at 100 °C for 24 h. Graphene sheets were prepared by thermal exfoliation of the graphite oxide in a muffle furnace at ∼1050 °C for ∼30 s.

2.3. Preparation of PA12 Nanocomposites. Prior to compounding, PA12 and graphene were dried at 80 °C under vacuum for 24 h. PA12 binary and ternary nanocomposites were prepared by melt compounding in a HAAKE MiniLab conical twin-screw extruder at 220 °C with a rotational speed of 80 rpm for 15 min under N_2 purge. The extrudates were compression-molded at 210 °C under 10 MPa to obtain specimens for testing. To study the effect of graphene location on morphology and electrical properties of the ternary nanocomposites, three compounding sequences were adopted:

T1: (PA12+graphene+POE-g-MA) (58/2/40) means that PA12, POE-g-MA, and graphene were melt-compounded simultaneously for 15 min.

T2: (PA12+graphene)+POE-g-MA (58/2/40) means that graphene was first compounded with PA12 for 10 min and then the resultant PA12/graphene nanocomposite was blended with POE-g-MA for 5 min.

T3: PA12+(graphene+POE-g-MA) (58/2/40) means that POE-g-MA was mixed with graphene for 5 min first and then the resulting POE-g-MA/graphene masterbatch was compounded with PA12 for 10 min.

In addition, PA12/POE-g-MA (58/40) binary blend was prepared under the same melt compounding condition, which is designated as NR. The prepared PA12/graphene binary nanocomposites with 1, 2 , and 3 wt % graphene are designated as B1, B2, and B3, respectively.

2.4. Characterization. A Philips CM12 transmission electron microscope (TEM) at an accelerating voltage of 100 kV was used to study the microstructures of graphene and its PA12 nanocomposites. Graphene sheets were dispersed in DMF by ultrasonication and collected on a standard TEM grid, while PA12 nanocomposites were cryogenically cut with a diamond knife at −100 °C for ultrathin sections thinner than 100 nm. As for the ternary nanocomposites, sections were then carefully stained with an aqueous solution of phosphotungstic acid and benzyl alcohol for 3−5 min to enhance the phase contrast between POE-g-MA and PA12. X-ray diffraction (XRD) patterns of PA12 nanocomposites were obtained on a Rigaku D/Max 2500 X-ray diffractometer (Japan) with CuKα radiation (λ = 1.54 Å) under a voltage of 40 kV and a current of 50 mA. The scanning was conducted with a speed of 5°/min from 3° to 35°. Direct current (DC) electrical conductivities of PA12 nanocomposites with higher conductivities than 10^{-6} S/m were measured by Keithley 4200-SCS (America) with a standard four probe method, while electrical conductivities of the nanocomposites and blends with lower conductivities than 1 × 10^{-6} S/m were measured by a ZC-90G

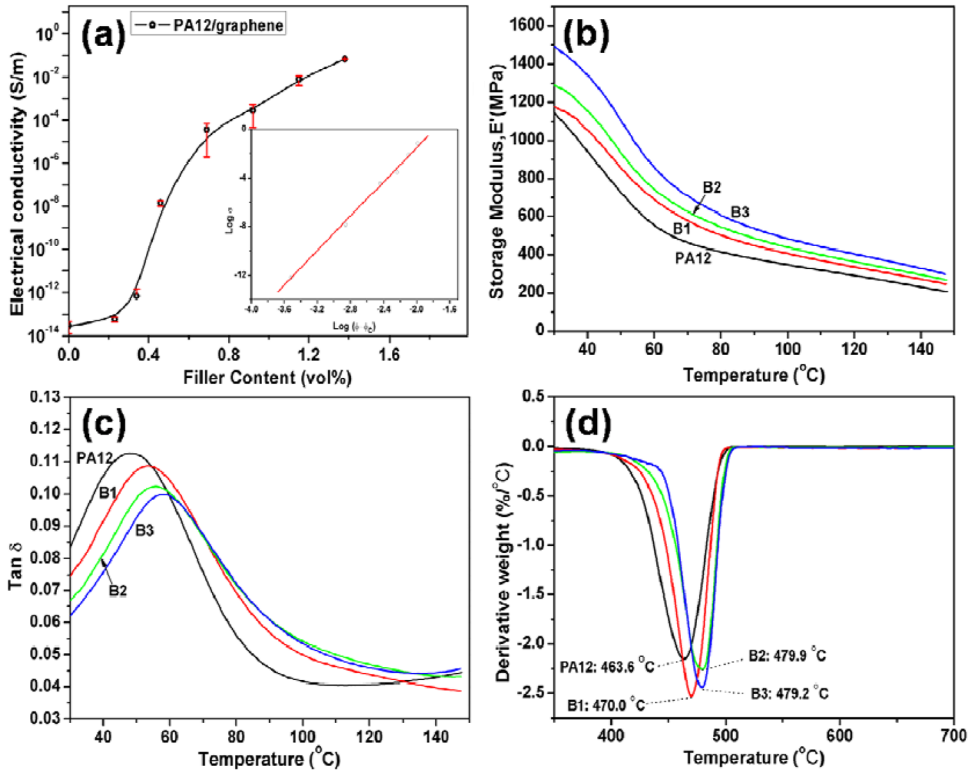

Figure 2. (a) Electrical conductivity versus graphene content for PA12/graphene nanocomposites. The inset is a double-logarithmic plot of electrical conductivity versus $(\varphi - \varphi_c)$; (b) storage modulus, (c) loss factor, and (d) TGA curves for neat PA12, (B1) PA12/1 wt % graphene, (B2) PA12/2 wt % graphene, and (B3) PA12/3 wt % graphene.

resistivity meter from Shanghai Taiou Electronics (China). All of the conductivity measurements were carried out at ambient temperature. Dynamic mechanical properties were measured with a TA-Q800 dynamic mechanical analyzer (DMA) using a tension mode at 1 Hz with a temperature ramp of 3 °C/min. Storage modulus and loss factor were obtained from room temperature to 150 °C for the binary nanocomposites and −100 to 150 °C for the ternary nanocomposites with POE-g-MA. Thermal properties were characterized by a Diamond Perkin-Elmer thermogravimetric analyzer (TGA) under nitrogen atmosphere at a heating speed of 10 °C/min from room temperature to 700 °C.

RESULTS AND DISCUSSION

Figure 1a shows the TEM image of graphene under low magnification. The transparent graphene sheet exhibits a wrinkled surface texture, which would improve its interactions with polymer matrix and facilitate its uniform dispersion.[1,2] Our previous results also indicate that each platelet is composed of ~3−4 individual graphene layers with an average thickness of ~1.2 nm.[2,5,9] To investigate the dispersion of graphene in PA12 matrix, the microstructure of the binary nanocomposite with 2 wt % graphene was characterized by TEM and XRD (Figure 1b−d). Graphene sheets were homogeneously distributed in PA12 matrix (Figure 1b and c). There was no new diffraction peak except for the three peaks of PA12 in the XRD patterns of the graphene nanocomposites (Figure 1d), suggesting the well-exfoliated state of graphene in the matrix. The crystalline structure of PA12 is pseudohexagonal γ form with peaks at 5.8° (020), 10.8° (040), and 21.5° (001).[31,32] The decrease in peak intensity with the increase of graphene content implies that the crystalline structure of PA12 became less perfect in the nanocomposites.[33]

The addition of graphene greatly improves the electrical conductivity of PA12 (Figure 2a). The PA12/graphene nanocomposites exhibit a rapid transition from electrically insulating to conducting with a low percolation threshold of 0.3 vol %, implying the formation of an interconnected graphene network for electrons transport throughout the matrix. This threshold value is even lower than that of graphene-filled polyethylene terephthalate (0.47 vol %) and polyurethane (>0.5 vol %) nanocomposites that were also prepared by melt compounding.[5,11] The electrical conductivity (σ) follows the power law at loadings near the percolation threshold (φ_c)[34,35]

$$\sigma \propto \sigma_0(\varphi - \varphi_c)^{\nu} \quad (1)$$

where σ_0 is the electrical conductivity of fillers, φ is the volume fraction of fillers above φ_c, and ν is the critical exponent describing the rapid variation of σ near percolation threshold. The percolation threshold is the critical content of fillers above which a continuous connected network is formed. As shown in the inset of Figure 2a for the double-logarithmic plot of σ versus $(\varphi-\varphi_c)$, the conductivities of PA12/graphene nanocomposites agree with the percolation behavior predicted by eq 1. When φ_c = 0.3 vol % and ν = 4.74, the straight line fits well with the experimental data. The nanocomposite with only 0.69 vol % graphene exhibits a high conductivity of 3.7×10^{-5} S/m, and the conductivity approaches to 6.7×10^{-2} S/m when the loading of graphene is 1.38 vol % (3 wt %). The efficiency of graphene in improving conductivity of PA12 is even higher than that of MWNTs. As demonstrated by Socher et al.,[36] PA12/MWNT nanocomposites prepared by melt compounding showed a higher percolation threshold of 0.9 wt %.

The wrinkled and folded feature of graphene was confirmed to enhance mechanical interlocking and load transfer with the

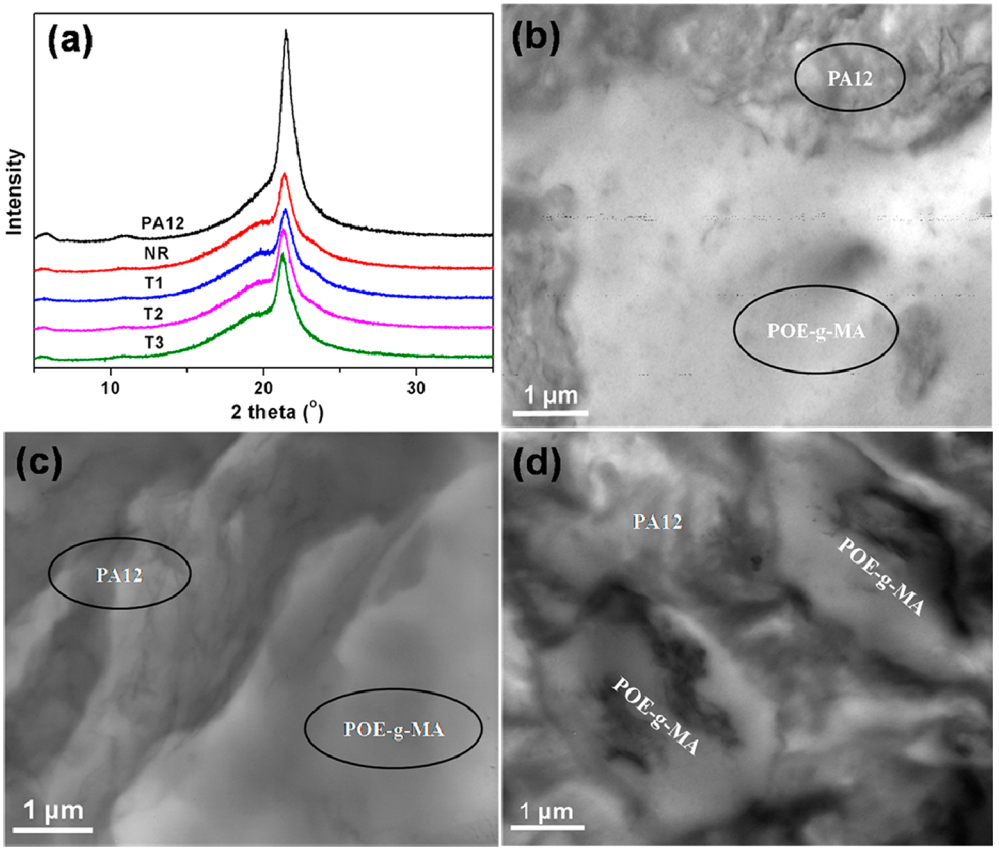

Figure 3. (a) XRD patterns of PA12 ternary nanocomposites with different compounding sequences; (b–d) TEM micrographs of the ternary nanocomposites of T1, T2, and T3, respectively.

matrix.[37] Panels b and c in Figure 2 are plots of storage modulus and loss factor versus temperature for neat PA12 and its graphene nanocomposites. The storage modulus increases with the increase of graphene content in the temperature range of 30–150 °C. At a given temperature of 30 °C, the storage modulus of PA12 is increased by 30% from 1.14 GPa of neat PA12 to 1.49 GPa for the nanocomposite with only 3 wt % graphene. The glass transition temperature (T_g) of PA12 is also improved because of the presence of graphene (Figure 2c). The addition of graphene also leads to a decrease in the area under the damping peak, indicating its stiffening effect to PA12 matrix.

The thermal stability of PA12/graphene nanocomposites was examined by TGA and the peak temperatures at which the mass loss rate is maximum (T_{max}) are given in Figure 2d. It is clear that the thermal stability of the PA12 nanocomposites is enhanced with increasing graphene content. With 2 wt % graphene, T_{max} is increased from 463.6 °C for neat PA12 to 479.9 °C for its nanocomposite. The enhanced thermal stability may benefit the improvement of flame retardancy of PA12.[38−40]

To further improve the electrical conductivity of the PA12/graphene nanocomposite, POE-g-MA was incorporated as the second polymer phase. XRD and TEM were used to evaluate the dispersion quality and location of graphene in the PA12/graphene/POE-g-MA ternary nanocomposites of T1, T2 and T3. The XRD patterns of the three ternary nanocomposites are similar to those of neat PA12 and its POE-g-MA binary blend and there are no diffraction peaks of graphene, indicating a good dispersion of graphene sheets (Figure 3a). However, the distribution states of graphene sheets are different in the three ternary nanocomposites (Figure 3b–d). In T1, graphene sheets are randomly dispersed in PA12 and POE-g-MA, and most sheets tend to distribute in PA12 matrix and only a few in POE-g-MA phase. While for T2, almost all the graphene sheets are preferentially located in PA12 matrix and there are no graphene sheets in the white rubber phase. In contrast, T3 exhibits a different microstructure from T1 and T2, graphene sheets are selectively located in white rubber phase with small aggregates. The aggregation may be induced by the high viscosity of the rubber, which limits the thermodynamic diffusion of polymer chains into the intragalleries of graphene and makes it difficult to break up the aggregates.

Figure 4 shows the effect of compounding sequence on the electrical conductivity of PA12/graphene/POE-g-MA ternary nanocomposites. The ternary nanocomposite of T1 exhibits almost the same electrical conductivity comparable to the binary nanocomposite of B2, which can be attributed to their similar graphene network formed in the matrix for electrons transport (Figure 3b). Reasonably, the ternary nanocomposite of T3 becomes electrically insulating even with the same loading of graphene. This is because graphene was first mixed with POE-g-MA before compounding with PA12, and thus it was mainly distributed in the isolated POE-g-MA phase. The graphene sheets located in the POE-g-MA phase are not able to form an interconnected network in PA12 matrix, which is responsible for the rather low electrical conductivity.

It is worth noting that the electrical conductivity of T2 is not only much higher than T1 and B2, but also higher than those of many other graphene-filled binary systems by melt compounding,[4,5,11] and even comparable to those of some systems

dx.doi.org/10.1021/am301119b | ACS Appl. Mater. Interfaces 2012, 4, 4740–4745

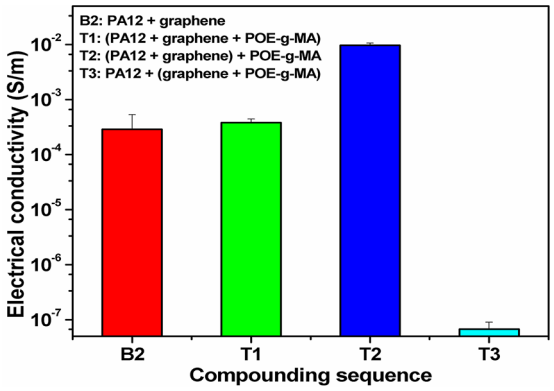

Figure 4. Effect of compounding sequence on electrical conductivities of PA12/2 wt % graphene/40 wt % POE-g-MA nanocomposites.

prepared by in situ polymerization and solution-mixing. The high electrical conductivity should be attributed to the volume-exclusion effect of POE-g-MA in T2,[12,22,41,42] where graphene sheets were selectively located in PA12 and a more compact conducting network was formed with the same loading of graphene (Figure 3c). The volume-exclusion effect was well applied to immiscible polymer blends, such as polystyrene/polyethylene/carbon black composites,[22] high density polyethylene/ultrahigh molecular weight polyethylene/graphite composites,[42] polyamide 6/POE-g-MA/carbon nanotube nanocomposites.[12] In addition, the use of POE-g-MA would be beneficial for the improvement of toughness of the conductive nanocomposites.[12,43]

Figure 5 shows the plots of storage modulus and loss factor of PA12/POE-g-MA/graphene nanocomposites as a function of temperature. In the temperature range below T_g of POE-g-MA (−100 to −50 °C), the storage moduli of neat PA12 and PA12/POE-g-MA binary blend are similar. However, the incorporation of graphene into PA12/POE-g-MA components greatly increases the storage modulus of the nanocomposites, indicating the reinforcement of graphene. In the temperature range above T_g of POE-g-MA (−50 to 150 °C), all the binary blend and ternary nanocomposites show a sharp decrease in storage modulus relative to neat PA12 because of the presence of POE-g-MA rubber. The slight differences of dynamic behavior for the three ternary nanocomposites may result from the selective location of graphene.

The glass transition relaxations of PA12 and POE-g-MA components can be distinctly recognized (Figure 5b). Neat PA12 exhibits two relaxation peaks, the α peak at 48.4 °C associated with the glass transition and the β peak at −66 °C due to segmental motion of the amide groups, which are not bonded to other amide groups,[44,45] whereas POE-g-MA shows only one glass transition peak at −38.9 °C. The relaxation temperatures of PA12, POE-g-MA, and their blend and nanocomposites are listed in Table 1. Compared to neat PA12 and PA12/POE-g-MA binary blend, the addition of graphene greatly enhances the T_g of PA12 in the three ternary nanocomposites. The increment in T_g of PA12 for T2 nanocomposite is higher than those of both T1 and T3, which is because the better reinforcement of graphene to PA12 in T2 due to the preferential localization of graphene in PA12 phase rather than in POE-g-MA. Owing to the chemical reactions during the melt extrusion,[45] the β relaxation peak of PA12 has disappeared. The T_g of POE-g-MA was shifted to low temperatures in its blend and ternary nanocomposites. The glass transition temperatures of PA12 and POE-g-MA for the ternary nanocomposites were affected by the localization of graphene sheets. Among the three ternary nanocomposites, T3 reveals the highest T_g of POE-g-MA because of the selective localization of graphene in POE-g-MA. The T_g of POE-g-MA in T2 is similar to that of PA12/POE-g-MA blend, and the T_g of POE-g-MA in T1 is in between of T2 and T3.

Table 1. DMA results of PA12, POE-g-MA, and their blend and nanocomposites

	PA12		POE-g-MA
composition	T_g(°C)	T_β(°C)	T_g(°C)
PA 12	48.4	−66.0	
POE-g-MA			−38.9
NR	49.5		−51.1
T 1	58.5		−49.4
T 2	61.0		−51.3
T 3	58.5		−45.2

CONCLUSIONS

Electrically conductive PA12/graphene nanocomposites with a low electrical percolation threshold of 0.3 vol % were prepared by melt compounding. The presence of graphene sheets improves the mechanical and thermal properties of PA12. POE-g-MA was used as the second polymer component to further enhance the electrical conductivity of PA12/graphene nano-

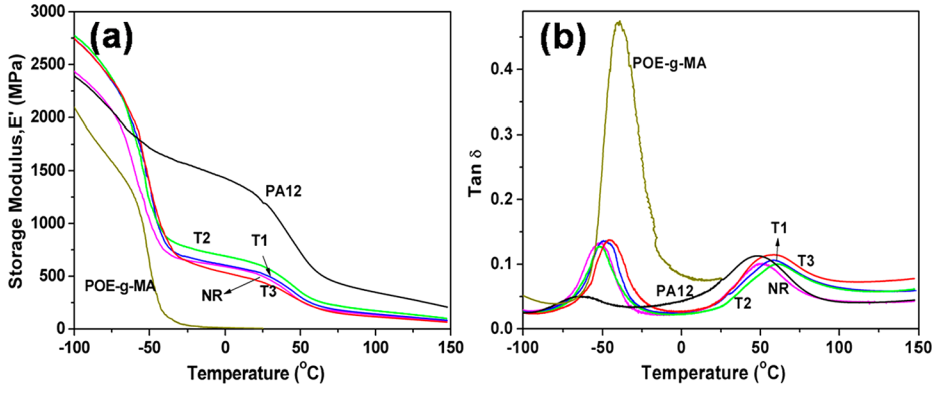

Figure 5. Effect of compounding sequences on (a) storage modulus and (b) loss factor of PA12/2 wt % graphene/40 wt % POE-g-MA nanocomposites.

composites. By varying the compounding sequences of PA12, graphene and POE-g-MA components, the location of graphene in the ternary nanocomposites was tailored. The distinct differences in electrical conductivity, storage modulus and glass transition temperatures for the ternary nanocomposites are attributed to the different localization of graphene. Both high electrical conductivity and storage modulus were obtained when most graphene sheets were located in PA12 matrix rather than in POE-g-MA phase.

AUTHOR INFORMATION

Corresponding Author

*Fax: +86-10-6442 8582; +86-10-8254 5586. E-mail: yuzz@mail.buct.edu.cn (Z.-Z.Y.); zhong.zhang@nanoctr.cn (Z.Z.).

Notes

The authors declare no competing financial interest.

ACKNOWLEDGMENTS

Financial support from the National Natural Science Foundation of China (51073012, 51103007, 51125010) is gratefully acknowledged.

REFERENCES

(1) Ramanathan, T.; Abdala, A. A.; Stankovich, S.; Dikin, D. A.; Herrera-Alonso, M.; Piner, R. D.; Adamson, D. H.; Schniepp, H. C.; Chen, X.; Ruoff, R. S.; Nguyen, S. T.; Aksay, I. A.; Prud'homme, R. K.; Brinson, L. C. *Nat. Nanotechnol.* **2008**, *3*, 327−331.

(2) Rafiee, M. A.; Rafiee, J.; Wang, Z.; Song, H. H.; Yu, Z. Z.; Koratkar, N. *ACS Nano* **2009**, *3*, 3884−3890.

(3) Yavari, F.; Rafiee, M. A.; Rafiee, J.; Yu, Z. Z.; Koratkar, N. *ACS Appl. Mater. Interfaces* **2010**, *2*, 2738−2743.

(4) Kim, H.; Miura, Y.; Macosko, C. W. *Chem. Mater.* **2010**, *22*, 3441−3450.

(5) Zhang, H. B.; Zheng, W. G.; Yan, Q.; Yang, Y.; Wang, J. W.; Lu, Z. H.; Ji, G. Y.; Yu, Z. Z. *Polymer* **2010**, *51*, 1191−1196.

(6) Yu, A.; Ramesh, P.; Sun, X.; Bekyarova, E.; Itkis, M. E.; Haddon, R. C. *Adv. Mater.* **2008**, *20*, 4740−4744.

(7) Kim, H.; Kobayashi, S.; AbdurRahim, M. A.; Zhang, M. J.; Khusainova, A.; Hillmyer, M. A.; Abdala, A. A.; Macosko, C. W. *Polymer* **2011**, *52*, 1837−1846.

(8) Yoonessi, M.; Gaier, J. R. *ACS Nano* **2010**, *4*, 7211−7220.

(9) Zhang, H. B.; Yan, Q.; Zheng, W. G.; He, Z.; Yu, Z. Z. *ACS Appl. Mater. Interfaces* **2011**, *3*, 918−924.

(10) Stankovich, S.; Dikin, D. A.; Dommett, G. H. B.; Kohlhaas, K. M.; Zimney, E. J.; Stach, E. A.; Piner, R. D.; Nguyen, S. T.; Ruoff, R. S. *Nature* **2006**, *442*, 282−286.

(11) Kim, H.; Macosko, C. W. *Polymer* **2009**, *50*, 3797−3809.

(12) Dasari, A.; Yu, Z. Z.; Mai, Y. W. *Polymer* **2009**, *50*, 4112−4121.

(13) Kim, J. Y.; Park, H. S.; Kim, S. H. *Polymer* **2006**, *47*, 1379−1389.

(14) Meng, H.; Sui, G. X.; Fang, P. F.; Yang, R. *Polymer* **2008**, *49*, 610−620.

(15) Steurer, P.; Wissert, R.; Thomann, R.; Mülhaupt, R. *Macromol. Rapid Commun.* **2009**, *30*, 316−327.

(16) Nguyen, D. A.; Lee, Y. R.; Raghu, A. V.; Jeong, H. M.; Shin, C. M.; Kim, B. K. *Polym. Int.* **2009**, *58*, 412−417.

(17) Pegel, S.; Pötschke, P.; Petzold, G.; Alig, I.; Dudkin, S. M.; Lellinger, D. *Polymer* **2008**, *49*, 974−984.

(18) Kodgire, P. V.; Bhattacharyya, A. R.; Bose, S.; Gupta, N.; Kulkarni, A. R.; Misra, A. *Chem. Phys. Lett.* **2006**, *432*, 480−485.

(19) Potschke, P.; Dudkin, S. M.; Alig, I. *Polymer* **2003**, *44*, 5023−5030.

(20) Hornbostel, B.; Potschke, P.; Kotz, J.; Roth, S. *Phys. Status Solidi B* **2006**, *243*, 3445−3451.

(21) Kim, H.; Macosko, C. W. *Macromolecules* **2008**, *41*, 3317−3327.

(22) Gubbels, F.; Jerome, R.; Teyssie, P.; Vanlathem, E.; Deltour, R.; Calderone, A.; Parente, V.; Bredas, J. L. *Macromolecules* **1994**, *27*, 1972−1974.

(23) Gubbels, F.; Blacher, S.; Vanlathem, E.; Jerome, R.; Deltour, R.; Brouers, F.; Teyssie, P. *Macromolecules* **1995**, *28*, 1559−1566.

(24) Gubbels, F.; Jerome, R.; Vanlathem, E.; Deltour, R.; Blacher, S.; Brouers, F. *Chem. Mater.* **1998**, *10*, 1227−1235.

(25) Thongruang, W.; Spontak, R. J.; Balik, C. M. *Polymer* **2002**, *43*, 3717−3725.

(26) Meincke, O.; Kaempfer, D.; Weickmann, H.; Friedrich, C.; Vathauer, M.; Warth, H. *Polymer* **2004**, *45*, 739−748.

(27) Yang, H.; Li, B.; Zhang, Q.; Du, R.; Fu, Q. *Polym. Adv. Technol.* **2009**, *22*, 857−862.

(28) Wu, G.; Li, B.; Jiang, J. *Polymer* **2010**, *51*, 2077−2083.

(29) Schniepp, H. C.; Li, J. L.; McAllister, M. J.; Sai, H.; Herrera-Alonso, M.; Adamson, D. H.; Prud'homme, R. K.; Car, R.; Saville, D. A.; Aksay, I. A. *J. Phys. Chem. B* **2006**, *110*, 8535−8539.

(30) McAllister, M. J.; Li, J. L.; Adamson, D. H.; Schniepp, H. C.; Abdala, A. A.; Liu, J.; Herrera-Alonso, M.; Milius, D. L.; Car, R.; Prud'homme, R. K.; Aksay, I. A. *Chem. Mater.* **2007**, *19*, 4396−4404.

(31) Owen, A. J.; Koliross, P. *Polym. Commun.* **1983**, *24*, 303−306.

(32) Wang, D.; Shao, C.; Zhao, B.; Bai, L.; Wang, X.; Yan, T.; Li, J.; Pan, G.; Li, L. *Macromolecules* **2010**, *43*, 2406−2412.

(33) Yoon, L. K.; Kim, B. K. *J. Appl. Polym. Sci.* **2000**, *78*, 1374−1380.

(34) Stauffer, D. *Introduction to Percolation Theory*; Taylor & Francis: London, 1985; pp 88−106.

(35) Kirkpatrick, S. *Rev. Mod. Phys.* **1973**, *45*, 574−588.

(36) Socher, R.; Krause, B.; Hermasch, S.; Wursche, R.; Pötschke, P. *Compos. Sci. Technol.* **2011**, *71*, 1053−1059.

(37) Rafiee, M. A.; Rafiee, J.; Srivastava, I.; Wang, Z.; Song, H.; Yu, Z.-Z.; Koratkar, N. *Small* **2010**, *6*, 179−183.

(38) Agag, T.; Koga, T.; Takeichi, T. *Polymer* **2001**, *42*, 3399−3408.

(39) Qin, H.; Zhang, S.; Zhao, C.; Hu, G.; Yang, M. *Polymer* **2005**, *46*, 8386−8395.

(40) Ye, L.; Wu, Q.; Qu, B. *Polym. Degrad. Stab.* **2009**, *94*, 751−756.

(41) Kotaki, M.; Wang, K.; Toh, M. L.; Chen, L.; Wong, S. Y.; He, C. *Macromolecules* **2006**, *39*, 908−911.

(42) Thongruang, W.; Balik, C. M.; Spontak, R. *J. Polym. Sci., Part B: Polym. Phys.* **2002**, *40*, 1013−1025.

(43) Chiu, F.; Lai, S.; Chen, Y.; Lee, T. *Polymer* **2005**, *46*, 11600−11609.

(44) Yu, Z. Z.; Ou, Y. C.; Qi, Z. N.; Hu, G. H. *J. Polym. Sci., Part B: Polym. Phys.* **1998**, *36*, 1987−1994.

(45) Han, C. D.; Chuang, H.-K. *J. Appl. Polym. Sci.* **1985**, *30*, 2431−2455.